[17] ——, "BONSAI: 3-D object recognition using constrained search," *IEEE Trans. Pattern Anal. Machine Intell.*, vol. 13, no. 10, pp. 1066–1075, Oct. 1991.
[18] M. Seibert and A. M. Waxman, "Adaptive 3-D object recognition from multiple views," *IEEE Trans. Pattern Anal. Machine Intell.*, vol. 14, no. 2, pp. 107–124, Feb. 1992.
[19] W.-C. Lin and T.-W. Chen, "CSG-based object recognition using range image," in *Proc. 9th Int. Conf. Pattern Recognit.*, Rome, Italy, Nov. 14–17, 1988, pp. 99–103.
[20] ——, "Inferring CSG-based object representation from range image," in *Proc. Vision Interface'90*. Halifax, NS, Canada, May 14–18, 1990, pp. 173–180; extended version appeared in *Pattern Recognition: Architectures, Algorithms, and Applications*, R. Plamondon and H. D. Cheng, Eds. New York: World Scientific, 1991, pp. 355–379.
[21] P. J. Besl and R. C. Jain, "Segmentation through variable-order surface fitting," *IEEE Trans. Pattern Anal. Machine Intell.*, vol. 10, no. 2, pp. 167–192, Mar. 1988.
[22] S. H. Friedberg, A. J. Insel, and L. E. Spence, *Linear Algebra*. Englewood Cliffs, NJ: Prentice-Hall, 1979, pp. 420–426.
[23] B. Kolman and R. C. Busby, *Discrete Mathematical Structures for Computer Science*. Englewood Cliffs, NJ: Prentice-Hall, 1984, pp. 133–134, pp. 172.
[24] B. Parvin and G. Medioni, "A constraint satisfaction network for matching 3D objects," in *Proc. IEEE Int. Joint Conf. Neural Netw.*, Washington DC, vol. II, June 18–22, 1989, pp. 281–286.
[25] W. Li and N. M. Nasrabadi, "Object recognition based on graph matching implemented by a Hopfield-style neural network," in *Proc. IEEE Int. Joint Conf. Neural Netw.*, Washington DC, vol. II, June 18–22, 1989, pp. 287–290.
[26] W.-C. Lin, F.-Y. Liao, C.-K. Tsao, and T. Lingutla, "A hierarchical multiple-view approach to three-dimensional object recognition," *IEEE Trans. Neural Netw.*, vol. NN-2, no. 1, pp. 84–92, Jan. 1991.
[27] D. E. Van Den Bout and T. K. Miller, III, "Improving the performance of the Hopfield-tank neural network through normalization and annealing," *Biological Cybern.*, vol. 62, pp. 129–139, 1989.
[28] ——, "Graph partitioning using annealed neural network," *IEEE Trans. Neural Netw.*, vol. NN-1, no. 2, pp. 192–203, June 1990.
[29] S. Kirkpatrick, C. Gelatt, and M. Vecchi, "Optimization by simulated annealing," *Science*, vol. 220, pp. 671–680, May 13, 1983.
[30] D. D. Hoffman and W. A. Richards, "Parts of recognition," *Cognition*, vol. 18, pp. 65–96, 1984.
[31] I. Biederman, "Human image understanding: Recent research," *Comput. Vision, Graphics Image Processing*, vol. 32, pp. 29–73, 1985.

On the Location Error of Curved Edges in Low-Pass Filtered 2-D and 3-D Images

Piet W. Verbeek and Lucas J. van Vliet

***Abstract*—In our research, we study the location error of curved edges in two- and three-dimensional images after analog and digital low-pass filtering. The zero crossing of a second derivative filter is a well-known edge localization criterion. The second derivative in gradient direction (SDGD) produces a predictable bias in edge location towards the centers of curvature while the linear Laplace filter produces a shift in the opposite direction. Their sum called PLUS (PLUS = Laplace + SDGD) leads to an edge detector that finds curved edges one order more accurately than its constituents. This argument holds irrespective of the dimension. The influence of commonly used low-pass filters (such as the PSF originating from diffraction limited optics using incoherent light (2-D), the Gaussian filter with variable cutoff point (*D*-D), and the isotropic uniform filter (*D*-D)) has been studied.**

***Index Terms*—Edge detection, edge location, Laplace, second derivative in gradient direction, edge bias, low-pass filters, curved edges, edge accuracy, subpixel resolution, derivatives of Gaussian.**

I. Introduction

In industrial and biomedical applications of digital image processing accurate determination of edge position is a key issue. Edge definitions based on zero crossings of some second derivative of the grey values are common. We have studied how edge locations according to such definitions are affected by low-pass filtering.

The zero crossing of a second derivative is basically defined in the analog domain. The actual processing is digital (using a sampled version of the image) and is designed to approximate optimally the analog results. Our error analysis will be done in the analog domain. Only edge detectors that can be digitally implemented are considered.

Low-pass filtering plays a role at two stages of image analysis. First, optical analog low-pass filtering produces the bandwidth limitation that allows sampling; second, digital low-pass filtering is applied to combat noise. As far as the edge location error is concerned, the second type of filtering can be reduced to the first: digital low-pass filtering on a sampled bandlimited signal is equivalent to analog low-pass filtering just before sampling. Therefore, we shall first investigate how analog low-pass filtering affects the accuracy of edge location. Fully aware of its insufficiency as a bandlimiting filter and its suboptimality as a noise reducer, we shall start our analysis with the simple isotropic uniform filter, the pillball filter. At a later stage we shall build stacks of pillballs to form Gaussian filters.

II. Second Derivative Filters

Gradient based edge detectors use the fact that the modulus of the first derivative is maximal at the position of the steepest ascent or descent, defined to be the edge location. Seeking a maximum of the gradient is equivalent to finding the zero crossing of

Manuscript received February 4, 1992; revised November 15, 1993. This work was supported in part by the The Netherlands Foundation for Biomedical Research NWO-MW (Grant 900–538–016) and The Netherlands Project Team for Computer Science Research SPIN (Projects Three-Dimensional Image Analysis and Delft Intelligence Assembly Cell). Recommended for acceptance by Associate Editor R. Nevatia.

The authors are with the Pattern Recognition Group of the Faculty of Applied Physics, Delft University of Technology, Lorentzweg 1, 2628 CJ Delft, The Netherlands; e-mail: piet@ph.tn.tudelft.nl.

IEEE Log Number 9400030.

a second derivative. Both methods being very sensitive to noise they are usually accompanied by some kind of low-pass filtering which in its turn may introduce a localization error or "mixing" of neighboring edges. At the same time this low-pass filtering justifies digital implementation. Edge finding through Gaussian smoothing and second derivative filtering followed by zero crossings detection has become commonplace. Marr [1], [2], [3], based his filter choice upon Difference-of-Gaussians (DOG) functions hypothesized in low level human vision. Most authors have considered the problem of straight step edge detection, which is essentially 1-D and has edge confusion as the main problem.

Gaussian Low-Pass Filtering: Canny [4], [5] has proven that based upon three criteria the derivative of a Gaussian is a very good approximation to the numerically optimal edge detector for 1-D step edges disturbed by additive Gaussian noise. Lunscher [6] shows that according to the Dickey and Shanmugam criterion [7] the optimal filter is equal to the second derivative of a Gaussian up to a suitable cutoff frequency. Xu [8] studied the error probabilities of the same operator along a straight edge in the presence of noise. With a new localization criterion Tagare [9] shows that the derivative of a Gaussian is the optimal edge detector for 1-D step edges. Recently, Sarkar, and Boyer [10], [11] presented optimal infinite impulse response filters for gradient and zero crossing based edge detectors that are similar to first and second derivatives of Gaussians. All these methods are similar to a second derivative with Gaussian low-pass filtering. We can easily understand the Gaussian optimality realizing that high SNR asks a narrow frequency width while edge confusion is prevented by a spatially narrow width. A Gaussian filter minimizes the product of spatial and frequency widths [12].

Extension of second derivative edge detection to two or higher dimensions offers the choice among different second derivatives such as the Laplace operator and the second derivative in gradient direction (SDGD, also called the second directional derivative). Due to its mathematical properties (linearity, simple Fourier description, intrinsic rotation invariance) and simple digital approximation, the Laplace is popular in image processing [13], [14].

Laplace: Berzins [15], considering the Laplace operator as a simple and practical approximation of the SDGD, has studied the accuracy of Laplacian-of-Gaussian edge detectors in relation to spatial features such as the size of the edge, the curvature of the edge and sharp corners. He remarks that the SDGD is robust with respect to second order illumination nonuniformity along the edge.

Second Derivative in Gradient Direction: The SDGD, a nonlinear operator, can be expressed in first and second derivatives. Haralick [16] approximated the SDGD using derivatives of a cubic polynomial model approximation of the underlying grey level surface. The cubic fit is equivalent to different low-pass filters for different derivatives, so that Haralick's result cannot be interpreted as the SDGD of some linear shift-invariant low-pass filtered image. Clark [17] and Torre [18] used the SDGD in its analytical description. Very fast approximations of the SDGD can be obtained using local maximum and minimum filters (grey-scale dilation and grey-scale erosion) [19]–[22]. A quantitative evaluation between an analytical SDGD, a nonanalytical SDGD and the Marr–Hildreth operator [22] shows comparable performance on synthetic test images heavily disturbed by Gaussian noise. To use the Laplace or the SDGD makes a difference in the edge position measured in the case of low-pass filtered curved edges [18] especially near corners [15].

PLUS Operator: We will show that both the SDGD and Laplace give off-edge (biased) zero crossings on low-pass filtered curved edges, but *on opposite sides* of the true edge such that the summed operator PLUS $\equiv$ SDGD + Laplace changes sign much closer to the true edge location.

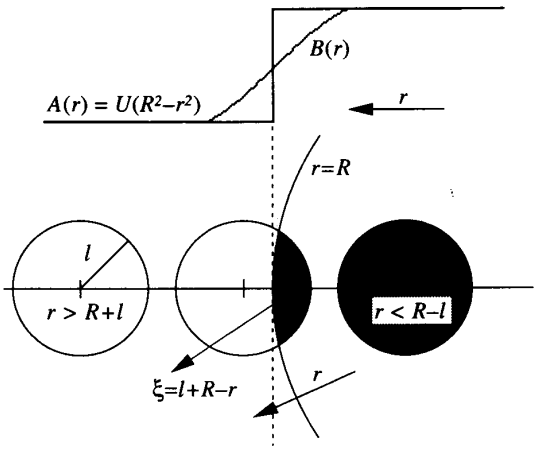

Fig. 1. Smoothing of a constant–curvature step edge by a single pillball filter.

We will derive estimates for the relative location error of the Laplace, the SDGD, and their sum "PLUS" as functions of the edge curvature and size of the smoothing filter. We give limits for the size of the smoothing filter with respect to the edge radius. Outside these limits (e.g. in the case of zero-radius corners) the accuracy cannot be guaranteed. Gaussian smoothing [15], and indeed any bandlimiting smoothing necessary for digital analysis always exceeds the zero-radius limit. For straight/planar edges *SDGD, Laplace* and *PLUS* all have on-edge zero crossing.

III. Spherical Step Edge Objects in High-Dimensional Space

We study the zero crossing position of step edge objects after low-pass filtering. Although the analysis will be carried out for the D-dimensional case, the figures will illustrate a two-dimensional example. In order to calculate the overlap area (volume in 3-D and hyper-volume in D-D) between a pillball filter and a step edge object we use the concept of integrated chord length (chord plane area in 3-D). The chord length $c(\xi, l, R)$ is a function of the overlap thickness ξ, the radius of the pillball l, and the radius of the object R (see Fig. 1). For planar edges we write $c(\xi, l, R) = c(\xi, l, \infty)$.

To analyze spherical objects it is convenient to use spherical coordinates. Take a spherical object of radius R, $A(r) = u(R^2 - r^2)$ where $u(\cdot)$ denotes the unit step function, $u(x) = 0$ if $x < 0$, $u(x) = 1$ if $x > 0$. $A(r)$ describes the (ideally sharp) analog image before low-pass filtering and $B(r)$ describes the image after low-pass filtering. The coordinate g is defined along the local gradient direction. The images that result from Laplace, SDGD, and PLUS operating on B are called *Laplace, SDGD,* and *PLUS*.

A. Smoothing by a Single Pillball

Smoothing image $A(r)$ with a pillball of radius l and height 1 gives a smoothed image $B(r)$ where r is the distance between the pillball center and the object center. $B(r) = b(r)$; if $r > R + l$ (pillball in 0-domain) $b(r) = 0$, if $r < R - l$ (pillball in 1-domain) $b(r) = \pi l^2$ (we assume the object larger than the pillball, $R > l$). If the pillball lies over the edge ($R - l < r < R + l$) the smoothed edge follows the rising overlap volume $O(r, l)$ between object and pillball. In 2-D the two intersection points of object edge and pillball edge span a chord with length c. In 3-D the ring of intersection points spans a circle, the chord plane, with diameter c and chord plane area C. In 4-D the intersection points span a sphere, in higher dimensions a hyper-sphere. Irrespective of the dimensionality for a spherical pillball intersecting a spherical object the diameter (called

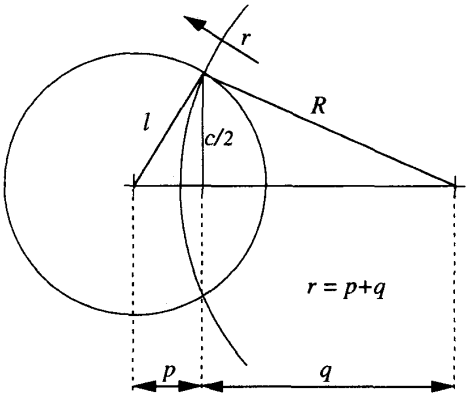

Fig. 2. A geometric sketch of a pillball intersecting a spherical object. Using $(\frac{c}{2})^2 + p^2 = l^2$, $(\frac{c}{2})^2 + q^2 = R^2$, $p + q = r$, we find an expression for the chord length as function of r, R, and l.

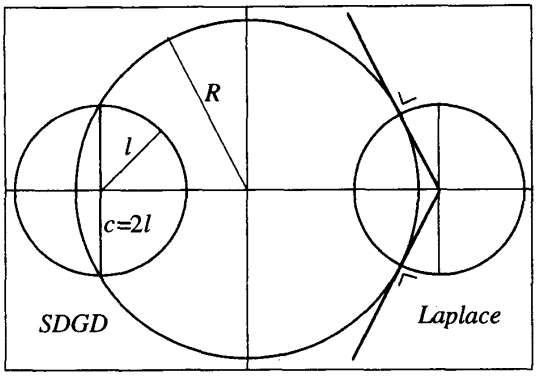

Fig. 3. Edge shifts produced by single pillball smoothing of a constant-curvature step edge for $k = 1/8$. The SDGD yields a zero-crossing when the chord is maximal. The Laplace yields a zero-crossing when the pillball and object boundary intersect at right angles.

chord length) is given by

$$c(\xi, l, R) = \sqrt{4l^2 - r^{-2}(r^2 - R^2 + l^2)^2} \tag{1}$$

with $r = l + R - \xi$. A geometric sketch that shows how to derive an expression of the chord length as a function of r, R, and l is given in Fig. 2. The corresponding chord plane area depends on the chord length and the dimensionality

$$C(D, c) = 2^{1-D} V(D-1) c^{D-1} \tag{2}$$

and $V(D)$ is the (dimensionless) volume of the D-dimensional sphere of radius 1.

$$V(D) = \pi^{D/2} / \Gamma\left(\frac{1}{2}D + 1\right). \tag{3}$$

The overlap $O(r, l)$ between the object and the pillball filter can be written as the integrated chord plane area $C(D, c(\xi, l, R))$ (cf. Fig. 1)

$$B(r) = O(r, l) = \int_0^{l+R-r} C(D, c(\xi, l, R)) d\xi. \tag{4}$$

The gradient direction is independent of l and always points towards the object center. The gradient magnitude of $B(r)$ is the chord plane area

$$B_g = -b_r = C. \tag{5}$$

Hence the *SDGD* is

$$SDGD = B_{gg} = b_{rr} = -C_r. \tag{6}$$

The *SDGD* crosses zero when the chord plane area C is maximal, when the pillball center lies in the chord plane. This occurs inside the curved object, thus off-edge. The Laplace is given by

$$Laplace = b_{rr} + (D-1)\frac{b_r}{r} = -C_r - (D-1)\frac{C}{r}. \tag{7}$$

For a planar step edge $R \to \infty$ and hence, $r \to \infty$. For planar edges Laplace and SDGD are identical and yield the same edge position. They have a zero crossing where the chord plane area C is maximal, i.e., when the pillball is exactly on-edge.

From (2), we have

$$C_r = 2^{1-D}(D-1)V(D-1)c^{D-2}c_r. \tag{8}$$

To find the zero crossing of *Laplace* and *SDGD*, we could insert (1), (2), (8) for c, C, and C_r into (6), (7) and solve for r, but it is simpler to use c^2 and r^2 instead. With $c_r = r/c\ \partial(c^2)/\partial(r^2)$

$$SDGD = -2^{1-D}(D-1)V(D-1)rc^{D-3}\left(\frac{\partial(c^2)}{\partial(r^2)}\right) \tag{9}$$

and

$$Laplace = -2^{1-D}(D-1)V(D-1)rc^{D-3}\left(\frac{\partial(c^2)}{\partial(r^2)} + \frac{c^2}{r^2}\right). \tag{10}$$

The zero crossing behavior of (9), (10) is governed by the factors between brackets which are independent of the dimensionality. The *SDGD* factor is $r^{-4}((R^2 - l^2)^2 - 1)$ and crosses zero if $r^2 = R^2 - l^2$. The *Laplace* factor is $2r^{-2}(R^2 + l^2 - r^2)$ and crosses zero for $r^2 = R^2 + l^2$, i.e., when pillball and circular object radii intersect at right angles (cf. Fig. 3). Hence the zero crossing of the *SDGD* is inside the object, on the center of the chord of length $2l$ (cf. Fig. 3), while the zero crossing of the *Laplace* is outside the object, on the intersection of the tangents at the ends of that chord. Both zero crossings are off-edge by a fraction of about $(l^2/2R^2)$ but in opposite directions.

The deviations from the actual edge position $r = R$ can be seen as relative errors in measured R of about $(l^2/2R^2) \equiv k$; for $R \to \infty$ the edge is planar with zero error, as discussed above; for a small object with, say $R = 2l$, the relative errors are 0.134 and 0.118 still well described by $k = \frac{1}{8}$. Due to the equal and opposite errors, a combination of *SDGD* and *Laplace* can be expected to give a more accurate location of the edge. The values of *SDGD* and *Laplace* at the edge are

$$SDGD|_{r=R} = (1-k)\frac{(D-1)}{2^{D-1}}\frac{4kR}{c^{3-D}} \tag{11}$$

$$Laplace|_{r=R} = -\frac{(D-1)}{2^{D-1}}\frac{4kR}{c^{3-D}}. \tag{12}$$

Consequently, the linear combination $SDGD + (1-k)\ Laplace$ crosses zero on-edge. This is of little use in cases when R is not exactly known. We propose to replace SDGD and Laplace by their sum, to be called PLUS

$$PLUS = 2b_{rr} + (D-1)\frac{b_r}{r} = -2C_r - (D-1)\frac{C}{r}$$
$$= -\frac{(D-1)V(D-1)r}{2^{D-1}c^{3-D}}\left(2\frac{\partial(c^2)}{\partial(r^2)} + \frac{c^2}{r^2}\right). \tag{13}$$

TABLE I
RELATIVE LOCATION ERROR FOR SINGLE PILLBALL FILTERS

SDGD	Laplace	PLUS
$\frac{r_0}{R}-1\approx -k=-\frac{l^2}{2R^2}$	$\frac{r_0}{R}-1\approx k=\frac{l^2}{2R^2}$	$\frac{r_0}{R}-1\approx \frac{k^2}{2}=\frac{l^4}{8R^4}$

We shall now show that PLUS locates the edge one order more accurately than its constituents. *PLUS* crosses zero for

$$r = r_0 = R\sqrt{\frac{1}{3}\left(1+2k+2\sqrt{1-2k+4k^2}\right)}. \tag{14}$$

Expanded to third order in k this gives

$$\frac{r_0}{R} = 1+\frac{1}{2}k^2+\frac{1}{2}k^3. \tag{15}$$

The relative location errors $(r_0 - R)/R$ are compared in Table I.

For a small object with $R = 2l$ $(k = \frac{1}{8})$ *PLUS* crosses zero at $r_0/R = 1.00876$, while $1+\frac{1}{2}k^2+\frac{1}{2}k^3 = 1.00879$ and $1+\frac{1}{2}k^2 = 1.00781$. The error is under 1% of R and is well described by $\frac{1}{2}k^2$. This is one order more accurate than either *SDGD* or Laplace that give an error of k. The absolute errors are $\pm kR = \frac{1}{2}l^2/R = \sqrt{k/2}l$ for Laplace and SDGD and $\frac{1}{2}k^2R = \frac{1}{8}l^4/R^3 = \sqrt{k^3/8}l$ for their sum PLUS (cf. Fig. 3). For a planar edge PLUS gives zero error, as expected from the behavior of SDGD and Laplace.

B. Smoothing by a Stack of Pillballs

Isotropic filters $h_{DD}(l)$ other than pillball filters can be handled as a stack of concentric pillballs. The cross section $h(l)$ will also be called the stack shape. Now consider a stack of concentric pillballs with height dh and monotonic radius distribution $l(h)$. The inverse function $h(l)$ is the stack shape; there is an $l_{\max}$ such that $h(l) = 0$ for $l > l_{\max}$. When the stack of pillballs crosses the edge, a smoothed image $B(r)$ results. In computing $B(r)$, we distinguish two situations: $-l_{\max} < r - R \le 0$ and $0 < r - R < l_{\max}$. Extension of (4) leads to a sum of overlap volumes $O(r,l)$ belonging to pillballs of different radii l. For an infinite number of pillballs this sum becomes an integral over h, or, with $dh = h_l dl$, over filter radius l (cf. Fig. 4). For $0 < r - R < l_{\max}$,

$$B(r) = \int_{|r-R|}^{l_{\max}} h_l O(r,l)dl, \tag{16a}$$

and for $-l_{\max} < r - R < 740$,

$$B(r) = \int_0^{|r-R|} h_l \pi l^2 dl + \int_{|r-R|}^{l_{\max}} h_l O(r,l)dl. \tag{16b}$$

The *SDGD* of the stack can be constructed from single pillball results, because the direction of grad $O(r,l)$ is independent of l and the l-integrated gradient has that same direction

$$\text{grad}\,(B(r)) = \int_{|r-R|}^{l_{\max}} h_l \,\text{grad}\,(O(r,l))dl. \tag{17}$$

Due to (2), (5) the single pillball results of (9)–(13) can all be written as

$$2^{1-D}(D-1)V(D-1)P(p,q,\rho^2,s,R) \tag{18}$$

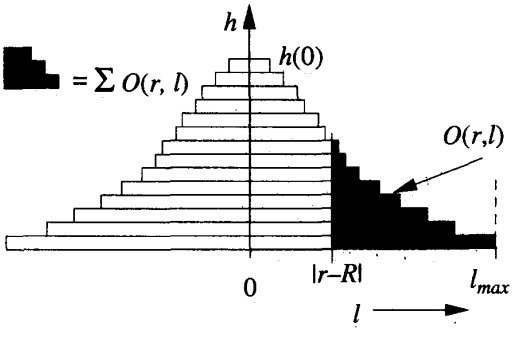

Fig. 4. Cross-section of a stack of pillballs partially overlapping a step edge. The smoothed image B equals the sum of the overlap area per pillball.

TABLE II
DEFINITIONS

	p	q	K	Ff^{D-3}	E	Gf^{D-5}
SDGD	1	0	$-\frac{1}{2}$	$1-\frac{1}{2}s^2$	0	$1-\frac{1}{4}(D+4)s^2+\frac{1}{8}(2D+3)s^4-\frac{1}{16}Ds^6$
Laplace	1	1	$\frac{1}{2}$	1	0	$1+\frac{1}{4}(D-2)s+\frac{1}{8}(D-2)s^4$
PLUS	2	1	$\frac{1}{8}$	1	2	$1-\frac{6}{8}s^2+\frac{1}{16}(D+5)s^4+\frac{1}{32}Ds^6$

with relative size $s \equiv l/R$ and relative position $\rho \equiv r/R$, with p and q according to Table II and

$$P\left(p,q,\frac{r^2}{R^2},\frac{l}{R},R\right) \equiv -rc^{D-3}\left(p\frac{\partial(c^2)}{\partial(r^2)}+q\frac{c^2}{r^2}\right). \tag{19}$$

The gradient direction is independent of l and the result of SDGD, Laplace, or PLUS for a stack of pillballs is given by an integral of single pillball results over radius l; in order to allow estimation of the zero crossing position we expand the integrand around $r = R$

$$\int_{|r-R|}^{l_{\max}} h_l P\left(p,q,\frac{r^2}{R^2},\frac{l}{R},R\right)dl \approx \int_{|\rho-1|}^{s_{\max}} h_s[P(p,q,1.s,R) + (\rho-1)P_\rho(p,q,1.s,R)]ds \tag{20}$$

where $h(s) \equiv h(l)$, with Taylor coefficients [23]

$$P(p,q,1,s,R) \equiv -2^D R^{D-2} g_1 f^{3-D} s^{D-1}$$
$$P_\rho(p,q,1,s,R) \equiv 2^D R^{D-2} g f^{5-D} s^{D-3}$$

and with correction factors $f \equiv (1-s^2/4)^{-1/2}$, $g_1 \equiv (2q-p)/4 + (p-q)s^2/8$ and

$$g \equiv p\left(\frac{1}{2}-\frac{4s^2}{8}+\frac{3s^4}{16}\right)+q\left(\frac{2s^2}{8}-\frac{s^4}{16}\right) + Dp\left(-\frac{s^2}{8}+\frac{2s^4}{16}-\frac{s^6}{32}\right)+Dq\left(\frac{2s^2}{8}-\frac{3s^4}{16}+\frac{s^6}{32}\right).$$

As the position of the zero crossing at $\rho = \rho_0$ lies outside the object for Laplace and PLUS, but inside the object for SDGD, $|\rho_0 - 1| = (2q-1)(\rho_0 - 1)$ and ρ_0 is the root of

$$\int_{(2q-1)(\rho_0-1)}^{s_{\max}} h_s P(p,q,1,s,R)ds + (\rho_0-1)\int_{(2q-1)(\rho_0-1)}^{s_{\max}} h_s P_\rho(p,q,1,s,R)ds = 0. \tag{21}$$

TABLE III
CHECKING LINEAR EXTRAPOLATION FOR SINGLE PILLBALL

	relative location error (lowest orders in s^2 or k)	$k=\frac{1}{8}, D=2$ approximation	$k=\frac{1}{8}, D=2$ exact
SDGD	$-\frac{1}{2}s^2\left(1+\frac{1}{4}(1+D)s^2\right) \equiv -k-\frac{1}{2}(1+D)k^2$	-0.1484	-0.1340
Laplace	$\frac{1}{2}s^2\left(1+\frac{1}{4}(1+D)s^2\right) \equiv k+\frac{1}{2}(1-D)k^2$	0.1172	0.1180
PLUS	$\frac{1}{8}s^4\left(1+\frac{1}{2}s^2\right) \equiv \frac{1}{2}k^2+\frac{1}{2}k^3$	0.00879	0.00876

TABLE IV
BOUNDS FOR M IF $0 < S < 1$

	2D			3D		
	M_{floor}	$M_{ceiling}$	$\frac{M_{ceiling}}{M_{floor}}$	M_{floor}	$M_{ceiling}$	$\frac{M_{ceiling}}{M_{floor}}$
SDGD	0.58	2.60	4.5	0.50	4	8
Laplace	0.65	1.15	1.8	0.67	1	1.5
PLUS	1	1.31	1.3	1	1.20	1.2

The relative error of the zero crossing position is thus

$$\rho_0 - 1 \approx K \int_0^\infty F h_s s^{D-1+E} ds \Big/ \int_0^\infty G h_s s^{D-3} ds \qquad (22)$$

with K, F, E and G defined according to Table II. One is free to set the upper integration boundary to $s_{\max}$.

For a check we apply this method to the single pillball case ($h_s \approx -\delta(s - s_0)$) and get for the approximate relative location error (indices 0 omitted)

$$\rho_0 - 1 \approx \frac{-P(p,q,1,s,R)}{P_\rho(p,q,1,s,R)} = K s^{2+E} \frac{F}{G} \qquad (23)$$

or, in both lowest orders in k the location errors given in Table III.

For the stack of pillballs prediction of the zero crossing position requires bounding of the two integrals in (22) [23]

$$\rho_0 - 1 \approx MK \int_0^{s_{\max}} h_s s^{D-1+E} ds \Big/ \int_0^{s_{\max}} h_s s^{D-3} ds \qquad (24)$$

with $M_{\text{floor}} < M < M_{\text{ceiling}}$, under the condition $h_s \leq 0$. For $D = 2$ and $D = 3$ the bounds M_{floor}, M_{ceiling} and their ratio are given in Table IV. The ratio $M_{\text{ceiling}}/M_{\text{floor}}$ indicates that for PLUS our argument allows the most accurate estimation of location error, both in 2-D and in 3-D, while for the SDGD the integral bounding method followed seems hardly applicable to estimate the behavior of the SDGD.

C. Gaussian Stack Shape

In order to study the accuracy of PLUS for a simple example we take the Gaussian filter and describe it as a stack of concentric pillballs. When the stack is on-edge the largest pillball at the base must properly intersect the object. Therefore, the Gaussian filter (unlimited support) is truncated at a radius of a few sigma ($a\sigma$) to become a finite impulse response filter (FIR).

$$h(l) = \left[\exp\left(-\frac{1}{2}l^2\sigma^{-2}\right) - \exp\left(-\frac{1}{2}a^2\right)\right] u(a\sigma - l). \qquad (25)$$

We take $a\sigma < R$ to guarantee proper intersection.

$$h_s = -\frac{R^2}{\sigma^2} s \exp\left(-\frac{1}{2}R^2 s^2 \sigma^{-2}\right) u(a\sigma - sR) \leq 0. \qquad (26)$$

As $h(l)$ (see (25)) is monotonous decreasing, the relative error in zero crossing position is (cf. (26)), $s_{\max} \equiv a\sigma/R$))

$$\rho_0 - 1 \approx MK\left(\frac{\sigma}{R}\right)^{2+E} \frac{I(D+E,a)}{I(D-2,a)} \qquad (27)$$

TABLE V
THE RELATIVE LOCATION ERROR $\rho 0 - 1$ FOR AN EDGE OF RADIUS R DUE TO LOW-PASS FILTERING BY A GAUSSIAN FILTER TRUNCATED AT $a\sigma < R$ ($a = 2$ AND $a \to \infty$)

	D	K	$\rho_0 - 1$ (a=2)	l_{eff}/σ (a=2)	$\rho_0 - 1$ ($a\to\infty$)	l_{eff}/σ ($a\to\infty$)
SDGD	2	$-\frac{1}{2}$	$-(0.25 \text{ to } 1.0)\frac{\sigma^2}{R^2}$	1.0 ±40%	$-(0.29 \text{ to } 1.3)\frac{\sigma^2}{R^2}$	1.0 ±40%
Laplace	2	$\frac{1}{2}$	$(0.35 \pm 30\%)\frac{\sigma^2}{R^2}$	0.8 ±15%	$(0.45 \pm 30\%)\frac{\sigma^2}{R^2}$	0.95 ±15%
PLUS	2	$\frac{1}{8}$	$(0.21 \pm 14\%)\frac{\sigma^4}{R^4}$	1.13 ±3%	$(0.43 \pm 14\%)\frac{\sigma^4}{R^4}$	1.36 ±3%
SDGD	3	$-\frac{1}{2}$	$-(0.33 \text{ to } 3.0)\frac{\sigma^2}{R^2}$	1.6 ±50%	$-(0.5 \text{ to } 4.0)\frac{\sigma^2}{R^2}$	1.9 ±50%
Laplace	3	$\frac{1}{2}$	$(0.57 \pm 20\%)\frac{\sigma^2}{R^2}$	1.05±10%	$(0.83 \pm 20\%)\frac{\sigma^2}{R^2}$	1.29 ±10%
PLUS	3	$\frac{1}{8}$	$(0.41 \pm 10\%)\frac{\sigma^4}{R^4}$	1.35 ±2%	$(1.1 \pm 10\%)\frac{\sigma^4}{R^4}$	1.72 ±2%

with $I(n,a)$ the nth moment of a truncated Gaussian (truncated at $a\sigma$)

$$I(n,a) \equiv \left(\frac{R}{\sigma}\right)^{n+1} \int_0^{a\sigma/R} \exp\left(-\frac{1}{2}R^2 s^2 \sigma^{-2}\right) s^n ds \qquad (28)$$

and with $M_{\text{floor}} < M < M_{\text{ceiling}}$, as long as $a\sigma/R < 1$. In [23] we derive the expressions for $I(0,a)$ to $I(5,a)$. The relative location errors for 2-D and 3-D Gaussian filters thus calculated are given in Table V. Also mentioned is the effective radius l_{eff}, the radius of the single pillball filter that yields the same error (see Table I). l_{eff} is found to be slightly larger than σ in most cases.

IV. SAMPLING

A sampling-invariant operation (SIO) is an Analog Operation $I_{\text{out}} = O_{\text{analog}}(I_{\text{in}})$ for bandlimited I_{in} and I_{out} which has a Discrete Counterpart Operation (DCO) that satisfies $\textit{Sampling}(I_{\text{out}}) = O_{\text{discrete}}(\textit{Sampling}(I_{\text{in}}))$ for sufficient band limitation of I_{in} [24]. The Laplace is such an SIO ($I_{\text{in}} = B$ and $I_{\text{out}} = \textit{Laplace}$ are bandlimited). Its DCO produces *Sampling (Laplace)* from which *Laplace* could be reconstructed and from which the *Laplace* zero crossings at the edge positions of the original disk A can be (subpixel) interpolated. The step edges characteristic for industrial images are thus located. SDGD and PLUS are no SIO's [24]. However, $|\text{grad}(\cdot)|^2$ SDGD$(\cdot)$ and $|\text{grad}(\cdot)|^2$ PLUS$(\cdot)$ are SIO's (for threefold bandwidth reduction). They shall be used instead, as $|\text{grad}(B)|^2$ *SDGD* and $|\text{grad}(B)|^2$ *PLUS* have the same zero crossing positions as *SDGD* and *PLUS*. We shall consider continuous 2-D and 3-D images and the impact of sampling on their analysis. The discretization of sample values to integers will not be considered.

A. Edge Location Error and Sampling Density

Applying Laplace to a bandlimited image sampled at the Nyquist rate doesnot require additional bandlimitation. A built-in Gaussian of $\sigma_{\text{derivative}} \geq 0.9$ will suffice. PLUS needs digital bandwidth reduction by a factor of three before digital implementation. This can be achieved by a built-in Gaussian of $\sigma_{\text{derivative}} \geq 2.7$. Moreover, the relative location error of Laplace is proportional to $\sim(\sigma/R)^2$ while the error of PLUS is proportional to $\sim(\sigma/R)^4$. Using this we find a break-even radius below which Laplace performs better than PLUS. The break-even radius is around $R = 6$ pixels. To guarantee proper intersection of the Gaussian filter and the spherical edge $R > 2\sigma$. This limits the applicability of PLUS to local radii larger than 5.4 pixels.

The above predicted errors are supported by an experiment (see the next section) where the radius of a disc runs from 10 pixels

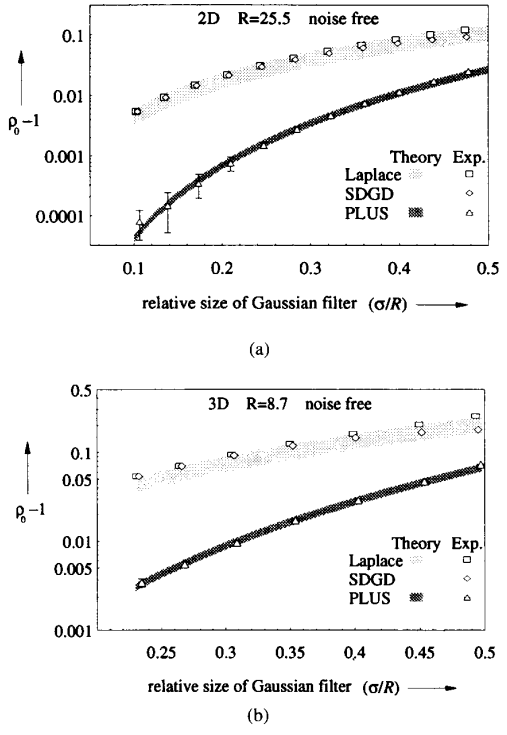

Fig. 5. Relative location error as function of the relative filter size in noise free images. The test images were sampled at the Nyquist rate.

down to 2 pixels for Laplace and down to 5.5 pixels for PLUS. The measurements shown in Fig. 6 are in full agreement with the error calculations in this section.

V. Experiments

A series of experiments were performed to test the theory presented in previous sections. In the following 2-D (3-D) experiments we have used a bandlimited disc of radius 25.5 (a bandlimited sphere of radius 8.7) as a test image. We have increased the resolution of the detection using cubic spline interpolation [25] to detect subpixel edge shifts. In all figures we have plotted the relative absolute location error as a function of the relative size (σ/R for the Gaussian filter). The prediction bands show the theoretical systematic error of Laplace and PLUS in noise free images. In experiment 1 and 3 all images were sampled at the Nyquist rate. Sampling at the Nyquist rate corresponds to a digital Gaussian filter of $\sigma_{\mathrm{PSF}} = 0.9$. The required threefold bandwidth reduction for SDGD and PLUS is achieved by digital low-pass filtering of the sampled image.

A. Implementation

We have used Gaussian derivatives to implement the Laplace, SDGD and PLUS. The overall Gaussian contains contributions of σ_{PSF}, σ_{smooth} and $\sigma_{\mathrm{derivatives}}$. Two times gradient filtering (derivative-of-Gaussian) yields a $\sqrt{2}$ times larger Gaussian filter than a true second derivative of Gaussian. Especially when we combine several first and second derivatives into a new filter (SDGD) we have taken special care that all built-in low pass filters (Gaussian kernels) have the same size (frequency response). If not, the new filter will be anisotropic.

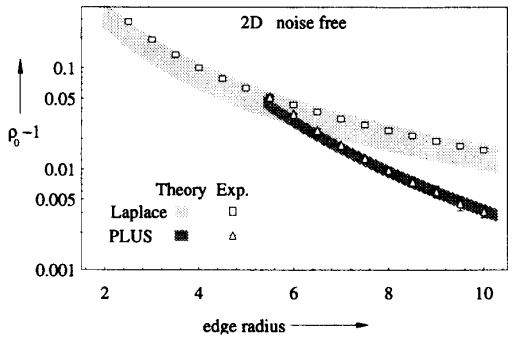

Fig. 6. Break-even radius between Laplace and PLUS for noise free 2-D images. Laplace was sampled without oversampling, PLUS with three times oversampling to avoid aliasing.

Noise Free Images (2-D and 3-D): We have tested the predicted location error for Gaussian filters in 2-D and 3-D. The test image was sampled at the Nyquist frequency. Proper digital low-pass filtering was used with SDGD and PLUS. Fig. 5 shows that the measured errors are in agreement with our prediction.

Break-Even Radius in 2-D: We have tested our prediction concerning the break-even point in the radius of the object where Laplace performs as well as PLUS (2-D). Note that PLUS needs three times oversampling when no digital low-pass filter is applied to combat noise. Laplace is satisfied by sampling at the Nyquist rate. These results are shown in Fig. 6 and confirm our prediction given in Section IV-A.

Robustness in the Presence of Noise (2-D and 3-D): In order to test the robustness of the edge detectors in the presence of noise we added independent Gaussian noise to the test images. SNR has been defined as the ratio between edge height (contrast) and the standard deviation of the noise in the image

$$\mathrm{SNR} = \frac{\text{edge height}}{\sigma_{\text{Gaussian noise}}}$$

or

$$\mathrm{SNR_{dB}} = 20 \log \left(\frac{\text{edge height}}{\sigma_{\text{Gaussian noise}}} \right). \tag{29}$$

For noisy images the relative absolute location error has two components, a systematic one and a stochastic one. The systematic error can be predicted as is shown in experiment 1. The stochastic error is responsible for the discrepancy between the measurements and the prediction bands in the Figs. 7 and 8.

VI. Conclusion

In this correspondence, we have shown that both analog and digital low-pass filters exert an influence on the location of curved edges in any dimension. The second derivative in the gradient direction produces a predictable bias in edge location towards the centers of curvature while the linear Laplace filter produces a shift in the opposite direction. We have shown that the sum of the above filters (PLUS = Laplace + SDGD) leads to an edge detector that finds the edges one order more accurately than its constituents.

All isotropic, monotonically-decreasing low-pass filters can be modeled by a concentric stack of pillballs and analyzed using the presented theory. This work describes the systematic errors in edge location which cannot be avoided. In the literature, mainly stochastic disturbances have been studied so far. (Optimal detection schemes have been presented for a planar step edge which is in principle a 1-D problem.) Low-pass filtered curved edges in any dimension produce

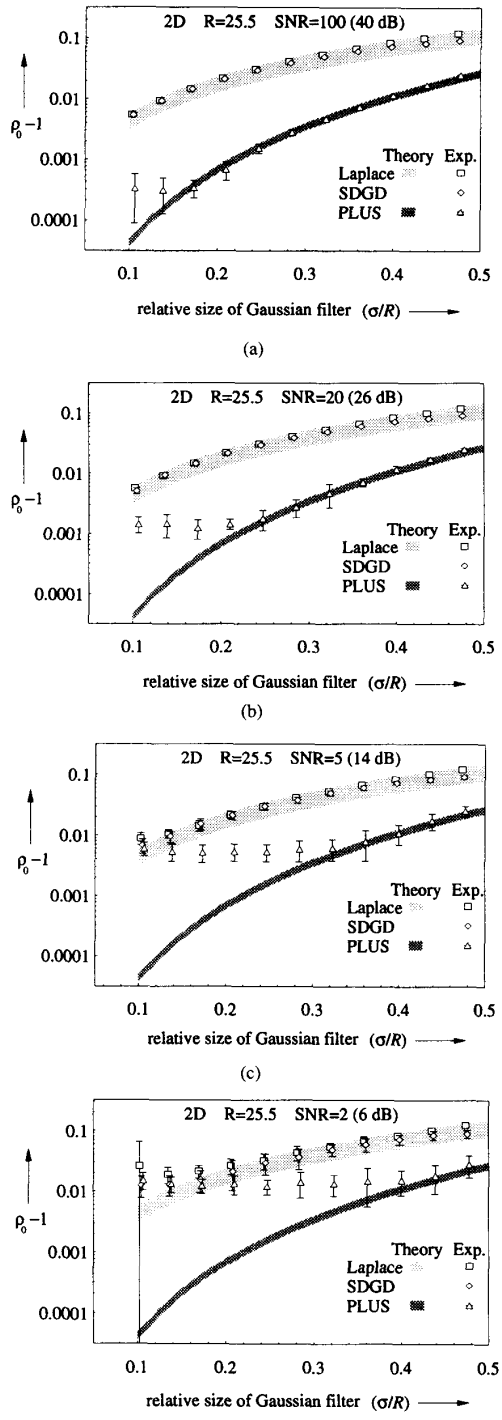

Fig. 7. Relative location error as function of the relative filter size for various SNR's with a Gaussian filter for noise reduction in 2-D. The test image was a disc of radius 25.5 pixels sampled at the Nyquist rate. The SNR's used are: a) SNR = 100 (40 dB), b) SNR = 20 (26 dB), c) SNR = 5 (14 dB), d) SNR = 2 (6 dB).

a biased zero-crossing (i.e., edge location) in a way that cannot be predicted from earlier results.

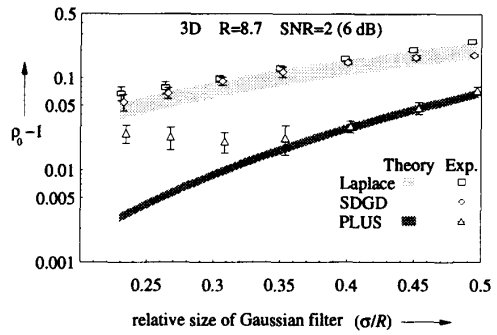

Fig. 8. Relative location error as function of the relative filter size for SNR = 2 (6 dB) with a Gaussian filter for noise reduction in 3-D. The test images were sampled at the Nyquist rate.

We have shown that PLUS (Laplace + SDGD) performs better than both its constituents over a wide range of SNR's and for a wide range of edge curvatures. The PLUS operator requires threefold oversampling when no digital smoothing is applied. The PLUS operator is easy to implement using separable filters, is isotropic, and allows interpolation. The latter is of extreme importance since it allows us to achieve subpixel accuracies. This is often the only way to overcome limited sampling density since the pixel size of a CCD camera has a smallest size and lenses with higher magnification are sometimes not available (e.g., microscope objectives).

The applicability of PLUS depends on the SNR and the object size. In 2-D, the SNR's can be divided in three intervals.

1) SNR $\geq$ 20 (SNR $\geq$ 26 dB): High-Quality Images require the smallest possible low-pass filters that provide the necessary band limitation using PLUS. Although the location error for PLUS is larger than in the theoretical noise free case (impossible to obtain due to quantization into a fixed number of bits, camera readout noise, and Poisson noise) PLUS performs significantly better than Laplace and SDGD.
2) $3 \leq$ SNR $<$ 20 (10 dB $\leq$ SNR $<$ 26 dB): Medium-Quality Images require small low-pass filters for Laplace and SDGD and slightly larger low-pass filters for PLUS to achieve the best performance. PLUS gives a slightly better performance in terms of location error, but limits the maximum allowed curvature of the contour. Laplace is the better choice for high curvature objects (radii smaller than 6 pixels) while PLUS is to be preferred when the curvature becomes less.
3) $1 \leq$ SNR $<$ 3 (0 dB $\leq$ SNR $<$ 10 dB): Low-Quality Images require large low-pass filters to get better accuracy as well as precision. For small objects the maximum allowed low-pass filter might not be sufficient in noise suppression. The stochastic error will dominate the total position error and there is no need for using PLUS. SDGD is less sensitive to nonlinear illumination along the edge (low frequency noise) and performs better under these conditions. When the objects become larger (radii larger than 20 pixels) and the curvature reduces, PLUS performs better than Laplace and SDGD because large low-pass filters can be applied. Although the difference is less than an order of magnitude, the edge displacement can now be reduced from a few pixels to less than one pixel.

For objects where the size of the low-pass filter is larger than the edge radius, no prediction with respect to edge location errors can be made. For contours having radii smaller than the break-even radius ($R_{\text{break-even}} = 6$) Laplace performs better than PLUS. For low SNR's the stochastic error dominates the total position error. For radii larger than the break-even radius, the SNR is the most dominant

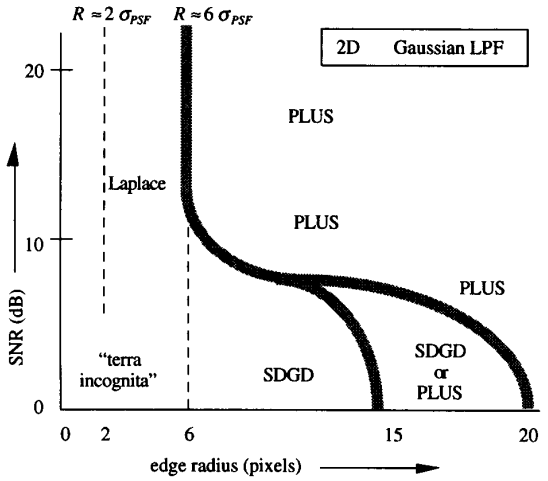

Fig. 9. Applicability domains of PLUS, Laplace, and SDGD as function of edge radius and SNR in 2-D.

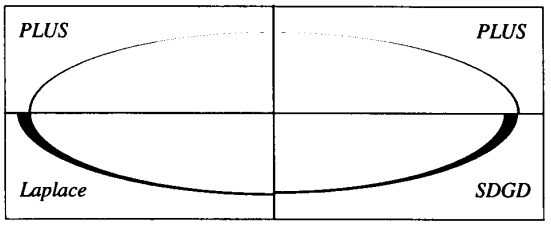

Fig. 10. Edge shifts produced by PLUS, Laplace, and SDGD on an ellipse, an object with slowly varying curvature.

feature for choosing the proper edge detector. Small objects (radii smaller than 6 pixels) heavily disturbed by noise cannot be localized using Laplace. Fig. 9 indicates which edge detector gives the best performance as function of the edge radius and the SNR in 2-D. In 3-D, small Gaussian filters are already very effective in noise reduction. This extends the applicability of PLUS to objects with smaller edge radii heavily disturbed by noise. Fig. 10 shows the edge shifts produced by PLUS, Laplace and SDGD on an ellipse, an object with slowly varying curvature.

REFERENCES

[1] D. Marr and E. C. Hildreth, "Theory of edge detection," in *Proc. Roy. Soc. Lon. B*, vol. 207, 1980, pp. 187–217.
[2] D. Marr and T. Poggio, "A theory of human stereo vision," in *Proc. Roy. Soc. Lon. B*,, vol. 204, 1979, pp. 301–328.
[3] E. C. Hildreth, "The detection of intensity changes by computer and biological vision systems," *Comput. Vision, Graphics and Image Processing*, vol. 22, pp. 1–27, 1983.
[4] J. Canny, "Finding edges and lines in images," M.S. thesis, M.I.T. Cambridge, MA, 1983.
[5] ——— "A computational approach to edge detection,"*IEEE Trans. Pattern Anal. Machine Intell.*, vol. PAMI-8, no. 6, pp. 679–698, 1986.
[6] W. H. H. J. Lunscher and M. P. Peddoes, "Optimal edge detector design I & II," *IEEE Trans. Pattern Anal. Machine Intell.*, vol. PAMI-8, no. 2, pp. 164–187, 1986.
[7] F. M. Dickey and K. S. Shamugan, "Optimal edge detection filter," *Appl. Opt.*, vol. 16, no. 1, pp. 145–148, 1977.
[8] Z. Xu, "A further study on error probabilities of Laplacian-Gaussian edge detection," in*8th Int. Conf. on Pattern Recognit.*, Paris, France, 1986, pp. 601–603.
[9] H. D. Tagare and R. J. P. DeFigueiredo, "On the localization performance measure and optimal edge detection," *IEEE Trans. Pattern Anal. Machine Intell.*, vol. 12, no. 12, pp. 1186–1190, 1990.
[10] S. Sarkar and K. L. Boyer, "On optimal infinite impulse response edge detection filters," *IEEE Trans. Pattern Anal. Machine Intell.*, vol. 13, no. 11, pp. 1154–1171, 1991.
[11] ———, "Optimal infinite impulse response zero crossing based edge detectors," *CVGIP: Image Understanding*, vol. 54, no. 2, pp. 224–243, 1991.
[12] A. Papoulis, *Signal Analysis*. New York: McGraw–Hill, 1977.
[13] A. Huertas and G. Medioni, "Detection of intensity changes with subpixel accuracy using Laplacian– Gaussian masks," *IEEE Trans. Pattern Anal. Machine Intell.*, vol. PAMI–8, no. 5, pp. 651–664, 1986.
[14] J. S. Chen, A. Huertas, and G. Medioni, "Fast convolutions with Laplacian–of–Gaussian masks," *IEEE Trans. Pattern Anal. Machine Intell.*, vol PAMI-9, no. 4, pp. 584–590, 1987.
[15] V. Berzins, "Accuracy of Laplacian edge detectors," *Comput. Vision, Graphics and Image Processing*, vol. 27, pp. 195–210, 1984.
[16] R. M. Haralick, "Digital step edges from zero crossing of second directional derivatives," *IEEE Trans. Pattern Anal. Machine Intell.*, vol. PAMI–6, no. 1, pp. 58–68, 1984.
[17] J. J. Clark, "Authenticating edges produced by zero-crossing algorithms," *IEEE Trans. Pattern Anal. Machine Intell.*, vol. 11, no. 1, pp. 43–57, 1989.
[18] V. Torre and T. Poggio, "On edge detection," *IEEE Trans. Pattern Anal. Machine Intell.*, vol. PAMI-8, no. 2, pp. 147–163, 1986.
[19] A. L. D. Beckers, "Parameter estimation for nonlinear object size filters in images," Master's thesis, (in Dutch) Faculty of Applied Physics, Delft Univ. of Technology, The Netherlands, 1986.
[20] J. Bernsen, "Dynamic thresholding of grey-level images," in *8th Int. Conf. Pattern Recognit.*, Paris, France, 1986, pp. 1251–1255.
[21] L. J. van Vliet, I. T. Young , and A. L. D. Beckers, "An edge detection model based on nonlinear Laplace filtering," in *Pattern Recognition and Artificial Intelligence—Towards an Integration*, E. S. Gelsema and L. N. Kanal, Eds. Amsterdam: Elsevier Science Publishers B. V. (North-Holland), 1988, vol. 7, pp. 63–73.
[22] ——— "A nonlinear Laplace operator as edge detector in noisy images," *Comput. Vision, Graphics, and Image Processing*, vol. 45, no. 2, pp. 167–195, 1989.
[23] L. J. van Vliet, "Grey-Scale Measurements in Multi-Dimensional Digitized Images," Ph.D. thesis, Delft Univ. Press, Stevinweg 1, Delft, The Netherlands, 1993.
[24] P. W. Verbeek, "A class of sampling-error free measures in oversampled band-limited images," *Pattern Recognit. Lett.*, vol. 3, pp. 287–292, 1985.
[25] W. H. Press, B. P. Flannery, S. A. Teukolsky, and W. T. Vetterling, *Numerical Recipes in C, The Art of Scientific Computing*. Cambridge, MA: Cambridge Univ. Press, 1990.